Journal of Sound and Vibration 433 (2018) 16–28

Contents lists available at ScienceDirect

Journal of Sound and Vibration

journal homepage: www.elsevier.com/locate/jsvi

Non-iterative, stable analysis of surface acoustic waves in anisotropic piezoelectric multilayers using spectral collocation method

Bo Lan

Department of Mechanical Engineering, Imperial College London, UK

ARTICLE INFO

Article history:
Received 7 December 2017
Revised 23 May 2018
Accepted 4 July 2018
Available online 14 July 2018
Handling Editor: G. Degrande

Keywords:
Surface acoustic waves
Piezoelectric multilayer
Spectral collocation method

ABSTRACT

Surface acoustic waves (SAWs) enjoy profound importance across many disciplines, and one of their most prominent applications are the vast ranges of SAW devices made of piezoelectric multilayers. Thus a stable and efficient algorithm of analysing key SAW parameters in arbitrary layered media is of wide interest. This paper introduces such an algorithm based on the spectral collocation method (SCM). It firstly explains the fundamental governing equations and their numerical calculations via the SCM in a self-contained way, and then demonstrates the technique on the well-studied ZnO/diamond/Si material system, where the key factors of phase velocity, electromechanical coupling coefficient and effective permittivity are evaluated and discussed in detail. Compared to the widely employed root-finding approach, it is shown that the SCM is intuitive to formulate and code, and is highly accurate; it delivers all modes at once, and does not suffer from numerical instabilities. The establishment of the method on this simple example also implies potential applications to more general material and geometry types that could be difficult for the conventional approaches.

1. Introduction

Derived by Lord Rayleigh to explain energy propagation in seismology [1], surface acoustic waves (SAWs) have since found wide-spread applications spanning from Earth Sciences [2] to non-destructive evaluations (e.g. detecting surface-breaking cracks [3] or recovering elastic properties [4]). Some of the most important and successful applications of SAW are in the areas of telecommunications and signal processing. Since 1960s, broad varieties and vast quantities (>3 billion annually as of 2007 [5]) of SAW-based devices have been manufactured, including bandpass filters, matched filters, resonators and delay lines, to name a few. These developments most dominantly relied on SAWs in piezoelectric crystals or deposited layers, using materials such as quartz and lithium niobate in early years, and later shifted to those with higher phase velocities (e.g. aluminium nitride and diamond) driven by the demands for higher-frequency devices [5,6]. Recently, SAWs in miniaturised piezoelectric systems have spurred fascinating research of accurate manipulation of microfluidics [7] and cells [8] in lab-on-a-chip, and highly sensitive Micro Electro-Mechanical Systems (MEMS) sensors [9].

Fundamental to all these applications is a stable, efficient and accurate way of analysing key SAW parameters, and many methods have been explored for this purpose. The classic Rayleigh method involved solving an eighth-order analytical characteristic equation at each trial value of a root-finding process [10], hence was computationally very expensive. Its usage was largely replaced by the transfer matrix method (TMM, proposed by Thomson [11] for guided waves, and was subsequently

E-mail address: bo.lan@imperial.ac.uk.

https://doi.org/10.1016/j.jsv.2018.07.007

applied on various SAW scenarios in Refs. [12–14]), which reshaped the analytical equations into eigenvalue problems of the characteristic matrices, for the benefits of greatly reduced computational difficulty and cost, thus earned itself wide-spread and long-lasting popularities. However, it is now well-known that in the case of large frequency-thickness combinations, the TMM suffers from numerical instabilities caused by its indiscrimination of all exponential partial waves within the layer (known as the large *fd* problem in the fields of guided waves [15]). Techniques proposed to amend this drawback include most notably the global matrix [16], surface impedance [17], scattering matrix [18] and recursive asymptotic stiffness matrix (RASM) [19] methods. While they successfully circumvent the instability problem in their own ways, all of these methods generally belong to the category of the root-finding approach, which can be difficult to implement, and modes could be easily missed if great care is not taken; and if the displacement or stress profiles along depth are of interests, additional steps of substituting the roots back and solving the resultant characteristic equations are needed.

Alternative to these 'exact', partial wave-based methods, numerical techniques have also been applied to study guided waves, such as the Semi-Analytical Finite Element (SAFE) method [20] and the spectral methods of polynomial expansion [21–23]. SAFE discretizes the cross section of the waveguide with finite or spectral elements in search for the solution to the wave equation. Its unique strength lies in its capability of modelling structures of arbitrary cross-section and elastic symmetry, but the relative complexity of the SAFE formulation appear an overkill for SAW applications, where the waveguides are normally of simple and regular geometries. The spectral methods, on the other hand, are of great practical value in this territory. They approximate the displacements along depth of a regular-shaped waveguide as series expansions of spectral bases such as the trigonometric, Legendre or Laguerre polynomials, which effectively reduce the wave equation into one-dimensional numerical partial differential equation, and avoids the erroneous growing exponential partial waves of large *fd* products and ensuring stability. Even though these expansions are not exact, the maintained numerical accuracy is so high that the inexactness is negligible [24]. The applications of the Legendre-Laguerre polynomial expansion method on guided wave studies are discussed in Refs. [23,25], and it is shown that different modes of the guided wave are obtained simultaneously from a generalised eigenvalue formulation, and that it is guaranteed that no mode will be missed. These papers also briefly touched on SAWs, but only briefly to the extent of calculating phase velocity and particle displacements.

The drawback of the spectral polynomial technique is that the expansion and reconstruction of displacement makes it somewhat cumbersome to apply boundary conditions and interpret results. The spectral collocation method (SCM) is in many ways an improvement over the explicit polynomial technique, and is particularly suitable for guided wave calculations. Here the explicit series expansion and reconstruction processes are hidden backstage in the form of differential matrices, and the function values are evaluated and used directly at the discrete collocation points. So not only all advantages of the conventional spectral methods are inherited, the characteristic SCM wave equation is also more straightforward to formulate and code, the SAW boundary conditions are simpler to prescribe, and mode profiles (e.g. displacements and stress) are directly obtained. Such benefits have been successfully demonstrated using SCM based on Chebyshev polynomials, on guided waves in isotropic [24], generally anisotropic [26–28] and viscoelastic [29] materials, in both Cartesian and cylindrical coordinate systems.

Given the advantages of the SCM, it is only logical to import it to the broad applications of SAW, but this has not been reported to the author's knowledge, nor has a full account of SAW characteristics based on spectral methods been given. The main contributions that this paper seeks to make to the literature, therefore, are firstly to set up a framework for employing the SCM (which is established for guided waves in elastic media) on the analysis of Rayleigh-type SAWs in anisotropic piezoelectric multilayers, with its extension to magneto-electro-elastic media given; and secondly it provides a demonstration of the method via a comprehensive analysis of key SAW performance parameters in an exemplary multilayer system. It is structured as follows: in Section 2, the analytical wave equation is introduced and reshaped into the simple, general matrix formulation; Section 3 lays out the basic idea of SCM, which transforms the nonlinear wave equation into a linear eigenvalue problem, before prescribing the SAW boundary conditions and solving it. As a demonstrative example, the multilayer system of ZnO/diamond/Si is analysed in Section 4, and all the key parameters for SAW applications are evaluated using the SCM.

2. Theoretical formulation

2.1. Multilayer system configuration

We consider the classic multilayer configuration shown in Fig. 1. The structure consists of n layers that occupy the space of $x_3 < 0$ to infinity, with the 1st layer at the top, and subsequent indices increasing with depth. Some of the layers can be non-piezoelectric (e.g. diamond), but there must be a piezoelectric one attached to metal electrodes (such as the interdigital transducer, IDT) to allow SAWs to be induced into and detected from the system.

The induced wave propagates along the x_1 direction. The medium is considered infinitely long along x_2, therefore the propagation can be seen as a two-dimensional problem on the $x_1 - x_3$ plane, with all physical variables independent of x_2. The wave field in each layer can be fully described by the generalised displacement vector $\mathbf{u} = [u_1, u_2, u_3, \phi]^{\mathrm{t}}$ and stress component vector $[\sigma_{31}, T_{32}, T_{33}, D_3]^{\mathrm{t}}$, where u_j are mechanical displacements, ϕ is the electrical potential, T_{ij} are the stress tensor components, D_3 is the electrical displacement along x_3, and t in the superscript means transpose. All variables in $\mathbf{u}$ can be written in a harmonic description of:

$$u_j = U_j(x_3)\exp[\mathrm{i}(\omega t - kx_1)] \tag{1}$$

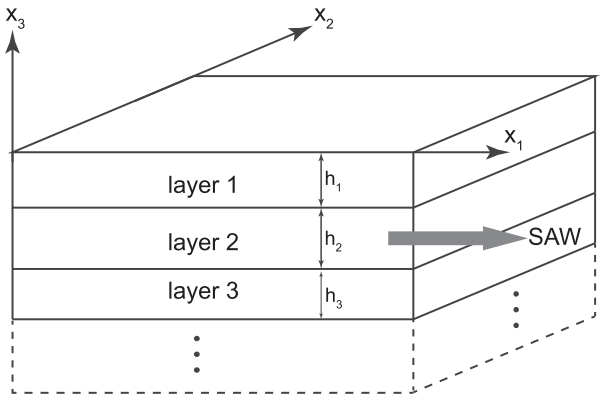

Fig. 1. Schematic of the wave propagation problem.

Obviously $\partial/\partial t = \mathrm{i}\omega$, $\partial/\partial x_1 = -\mathrm{i}k$ (i is the imaginary number), and $\partial/\partial x_2 = 0$. Note that u_2 and T_{32} are generally coupled with other variables for anisotropic media, thus must be included for the full description of the wave field, unless in cases of isotropy or $x_1 - x_3$ being a sagittal plane (e.g (100) of a cubic material).

A fixed coordinate system is adopted in this paper, with the SAW always propagating along x_1. For considerations along arbitrary crystallographic planes and directions, properties of the material, including the 4th-rank elastic, 3rd-rank piezoelectric, and 2nd rank permittivity tensors, need to be rotated into alignment with the $x_1 - x_2 - x_3$ system.

2.2. Fundamental governing equations

Wave propagations in the multilayer of Fig. 1 are governed [30] by the elastic and piezoelectric constitutive equations:

$$T_{ij} = c_{ijkl}\frac{\partial u_k}{\partial x_l} + e_{kij}\frac{\partial \phi}{\partial x_k} \tag{2a}$$

$$D_i = e_{ikl}\frac{\partial u_k}{\partial x_l} - \epsilon_{ik}\frac{\partial \phi}{\partial x_k} \tag{2b}$$

combined with the conservation of momentum equation when there is no body force or current density:

$$\nabla \cdot \mathbf{T} = \frac{\partial T_{ij}}{\partial x_j} = \rho\frac{\partial^2 u_i}{\partial t^2} \tag{3a}$$

$$\nabla \cdot \mathbf{D} = \frac{\partial D_i}{\partial x_i} = 0. \tag{3b}$$

In addition, SAWs also need to satisfy the free-stress mechanical boundary conditions:

$$T_{3j} = 0, j = 1, 2, 3, \text{ when } x_3 = 0. \tag{4}$$

and appropriate electrical (either open- or short-circuit) conditions at the top surface. Here ρ is the material density, and c_{ijkl}, e_{ijk} and ϵ_{ij} are the components of the elastic, piezoelectric and permittivity tensors, respectively. Einstein's summation convention over repeated subscripts are assumed throughout, e.g. $\partial T_{ij}/\partial x_j$ denotes a summation over j.

These equations summarise the physical relations rather concisely; for a more lucid formulation accessible by the SCM, notations used by the TMM are emulated to expand, for example, the first column of the stress tensor T_{i1} and the electrical displacement D_1 into:

$$T_{i1} = c_{i1k1}\frac{\partial u_k}{\partial x_1} + e_{1ij}\frac{\partial \phi}{\partial x_1} + c_{i1k3}\frac{\partial u_k}{\partial x_3} + e_{3ij}\frac{\partial \phi}{\partial x_3} \tag{5a}$$

$$D_1 = e_{1k1}\frac{\partial u_k}{\partial x_1} - \epsilon_{11}\frac{\partial \phi}{\partial x_1} + e_{1k3}\frac{\partial u_k}{\partial x_3} - \epsilon_{13}\frac{\partial \phi}{\partial x_3} \tag{5b}$$

Following the notation Γ^{mn} used in Refs. [13,14]:

$$\Gamma^{mn} = \begin{bmatrix} c_{1m1n} & c_{1m2n} & c_{1m3n} & e_{n1m} \\ c_{2m1n} & c_{2m2n} & c_{2m3n} & e_{n2m} \\ c_{3m1n} & c_{3m2n} & c_{3m3n} & e_{n3m} \\ e_{m1n} & e_{m2n} & e_{m3n} & -\epsilon_{mn} \end{bmatrix} \tag{6}$$

and taking advantage of the harmonic waves in Eq. (1) ($\partial/\partial t = \mathrm{i}\omega, \partial/\partial x_1 = -\mathrm{i}k$), Eq (5) can be combined into a compact matrix function of the generalised vector $\mathbf{u}$ as:

$$\begin{bmatrix} T_{i1} \\ D_1 \end{bmatrix} = \Gamma^{11}\frac{\partial}{\partial x_1}\mathbf{u} + \Gamma^{13}\frac{\partial}{\partial x_3}\mathbf{u} = (-\mathrm{i}k)\Gamma^{11}\mathbf{u} + \Gamma^{13}\frac{\partial}{\partial x_3}\mathbf{u} \tag{7}$$

Similarly, the 3rd column of the stress tensor T_{i3} and D_3 can be bound together as:

$$\begin{bmatrix} T_{i3} \\ D_3 \end{bmatrix} = \Gamma^{31}\frac{\partial}{\partial x_1}\mathbf{u} + \Gamma^{33}\frac{\partial}{\partial x_3}\mathbf{u} = (-\mathrm{i}k)\Gamma^{31}\mathbf{u} + \Gamma^{33}\frac{\partial}{\partial x_3}\mathbf{u} \tag{8}$$

Substituting the forms of Eqs (7) and (8) back into Eq. (3) leads to the wave equation:

$$[(-k^2)\Gamma^{11} - (\mathrm{i}k)(\Gamma^{13} + \Gamma^{31})\frac{\partial}{\partial x_3} + \Gamma^{33}\frac{\partial^2}{\partial x_3^2}]\mathbf{u} = -\rho\omega^2\mathbf{I}_p \cdot \mathbf{u} \tag{9}$$

where $\mathbf{I}_p$ is the 3×3 identity matrix augmented by a 4th column and 4th row of zeros. Note that the Γ matrices are capable of accounting for arbitrary anisotropy of the tensors, as well as viscoelastic effects that introduce imaginary parts to their values [29]. It is also worth noting that Eq. (9) is a general form with wider applicabilities to both the simpler, non-piezoelectric elastic media and the more complicated, magneto-electro-elastic cases. For the former, one only needs to remove all the electrical variables from the equation; and for the latter, the magnetic potential φ should be included in the generalised $\mathbf{u}$ to make it $[u_1, u_2, u_3, \phi, \varphi]^{\mathrm{t}}$, and as a result, the Γ matrices are expanded into [23]:

$$\Gamma^{mn} = \begin{bmatrix} c_{1m1n} & c_{1m2n} & c_{1m3n} & e_{n1m} & q_{n1m} \\ c_{2m1n} & c_{2m2n} & c_{2m3n} & e_{n2m} & q_{n2m} \\ c_{3m1n} & c_{3m2n} & c_{3m3n} & e_{n3m} & q_{n3m} \\ e_{m1n} & e_{m2n} & e_{m3n} & -\epsilon_{mn} & 0 \\ q_{m1n} & q_{m2n} & q_{m3n} & 0 & -\mu_{mn} \end{bmatrix} \tag{10}$$

where q_{ijk} and μ_{ij} are respectively the piezomagnetic stress constants and the magnetic permeability constants. Accordingly, the matrix $\mathbf{I}_p$ is further augmented by a fifth column and row of zeros.

Eq. (9) gives the matrix description of the wave equation that is applicable to many types of guided waves (e.g. Lamb waves [27,28]), depending on the specific boundary conditions prescribed. Those for the SAW will be introduced in the following section.

3. Numerical solutions

3.1. Discretization with spectral collocation method (SCM)

The SCM provides a simple and accurate tool for evaluating partial differentiate equations. Its most important idea is that in a confined region such as $x_3 \in [-1, 1]$, a function of x_3 continuous to the nth order can be expanded in terms of polynomials, so that at the discretized grids of the polynomials' collocation points, the nth-order differentiation values of the function can be accurately approximated by multiplying a pre-computed matrix - called the differentiation matrix (DM) - with the function values themselves. For example, the differentiation of the displacement component u_1 along x_3 can be calculated as:

$$\frac{\partial^{(n)}u_1}{\partial x_3^{(n)}} = \mathbf{Diff}^{(n)}\mathbf{U}_1 \tag{11}$$

where $\mathbf{Diff}^{(n)}$ is the nth order DM, and $\mathbf{U}_1$ are the values of u_1 at collocation points. For a bounded domain, the Chebychev grids are widely employed as the discretization scheme, and their DMs are easily generated to an arbitrary number of nodes N using an opensource toolbox [31]. Here the number N determines the expansion order with respect to the Chebychev polynomial bases, and both the accuracy and computational costs increase with N. Such DMs are usually in the interval of $x_3 \in [-1, 1]$, with the 1st node at the top ($x_3 = 1$), and the last (the Nth) node at the bottom ($x_3 = -1$); for a medium of arbitrary thickness h (i.e. $y \in [-h/2, h/2]$), the DM is obtained by mapping its values from x_3 to y:

$$y = x_3 \cdot \left(\frac{h}{2}\right) \Rightarrow \frac{\partial^{(n)}}{\partial y^{(n)}} = \frac{\partial^{(n)}}{\partial x_3^{(n)}}\frac{\partial^{(n)}x_3}{\partial y^{(n)}} = \frac{\partial^{(n)}}{\partial x_3^{(n)}} \cdot \left(\frac{2}{h}\right)^n \tag{12}$$

therefore:

$$\mathbf{Diff}^{(n)}_{[-\frac{h}{2},\frac{h}{2}]} = \mathbf{Diff}^{(n)}_{[-1,1]} \cdot \left(\frac{2}{h}\right)^n. \tag{13}$$

Note that the n over 2/h stands for power. Thus the differentiation operations are transformed into linear matrix multiplications that are easy to manipulate. The fundamental idea of discretising differential equations is similar to the familiar finite difference or finite element methods, but the interpolation scheme with the spectral polynomials are much more efficient and accurate [24].

3.2. The ω and k formulations

Through introducing the DMs and discretizing the Γ and $\mathbf{I}_p$ matrices accordingly (by replacing each element with itself multiplying the $N \times N$ identity matrix), both sides of Eq. (9) are simplified into the product of a matrix and a vector:

$$\mathbf{LU} = \omega^2 \mathbf{MU} \tag{14}$$

where $\mathbf{L}$ is a $4N \times 4N$ matrix whose values are dependent on the wavenumber k, $\mathbf{U}$ is a $4N \times 1$ vector containing the values of the vector $\mathbf{u}$ at the Chebyshev grids, and $\mathbf{M}$ is a $4N \times 4N$ matrix only dependent on material properties.

Apparently Eq. (14) can be used to obtain ω (and hence the SAW phase velocity) when k is known. In this case, once appropriate boundary conditions are prescribed into $\mathbf{L}$ and $\mathbf{M}$ (details later), the equation becomes a simple linear eigenvalue problem between the matrices, with ω^2 being the eigenvalue and $\mathbf{U}$ the eigenvector. Eq. (14) is henceforth referred to as the ω formulation of the wave equation.

There are often cases where ω (or the frequency f) is known, and k needs to be computed. Eqs (9) and (14) are inadequate for this since their left sides are a quadratic equation of k, preventing it from being obtained as the eigenvalue directly from linear operations. A simple trick of introducing an auxiliary vector $\mathbf{v} = k\mathbf{u}$, however, is enough to enable such solution (referred to as the companion matrix in Ref. [29]). Substituting it back to Eq. (9) and writing them together give:

$$k\Gamma^{11}\mathbf{v} + \left[(\mathrm{i}k)(\Gamma^{13} + \Gamma^{31})\frac{\partial}{\partial x_3}\right]\mathbf{u} = \left[\Gamma^{33}\frac{\partial^2}{\partial x_3^2} + \rho\omega^2\mathbf{I}_p\right]\mathbf{u} \tag{15a}$$

$$k\mathbf{u} = \mathbf{v} \tag{15b}$$

which are equivalent to the matrix form:

$$\begin{bmatrix} \Gamma^{33}\dfrac{\partial^2}{\partial x_3^2} + \rho\omega^2\mathbf{I}_p, & \mathbf{0} \\ \mathbf{0}, & \mathbf{I} \end{bmatrix}\begin{bmatrix}\mathbf{u}\\ \mathbf{v}\end{bmatrix} = k\begin{bmatrix} \mathrm{i}(\Gamma^{13} + \Gamma^{31})\dfrac{\partial}{\partial x_3}, & \Gamma^{11} \\ \mathbf{I}, & \mathbf{0} \end{bmatrix}\begin{bmatrix}\mathbf{u}\\ \mathbf{v}\end{bmatrix} \tag{16}$$

where $\mathbf{I}$ refers to the identity matrix (not to be confused with $\mathbf{I}_p$). The SCM can then be introduced to discretize Eq. (16) into an eigensystem with k as the eigenvalue:

$$\mathbf{L}'\mathbf{U}' = k\mathbf{M}'\mathbf{U}' \tag{17}$$

where $\mathbf{L}'$ and $\mathbf{M}'$ are both $8N \times 8N$ matrices, and $\mathbf{U}'$ is a $8N \times 1$ vector. Eq. (17) is referred to as the k formulation. Compared to Eq. (14), the necessary introduction of $\mathbf{v}$ to enable k as the eigenvalue is at a cost of lower computation efficiency, as the size of the matrices are doubled.

The two formulations only describe the wave equation within a single layer; for a multilayer structure, the overall matrices can be effortlessly assembled by stacking up the equations layer by layer from the top. For example, by using the ω formulation, one gets:

$$\begin{bmatrix} \mathbf{L}|_{l1} & \mathbf{0} & \dots & \mathbf{0} \\ \mathbf{0} & \mathbf{L}|_{l2} & \dots & \mathbf{0} \\ \vdots & \vdots & \ddots & \\ \mathbf{0} & \mathbf{0} & \dots & \mathbf{L}|_{\mathrm{ln}} \end{bmatrix}\begin{bmatrix}\mathbf{U}|_{l1}\\ \mathbf{U}|_{l2}\\ \vdots\\ \mathbf{U}|_{\mathrm{ln}}\end{bmatrix} = \omega^2\begin{bmatrix} \mathbf{M}|_{l1} & \mathbf{0} & \dots & \mathbf{0} \\ \mathbf{0} & \mathbf{M}|_{l2} & \dots & \mathbf{0} \\ \vdots & \vdots & \ddots & \\ \mathbf{0} & \mathbf{0} & \dots & \mathbf{M}|_{\mathrm{ln}} \end{bmatrix}\begin{bmatrix}\mathbf{U}|_{l1}\\ \mathbf{U}|_{l2}\\ \vdots\\ \mathbf{U}|_{\mathrm{ln}}\end{bmatrix}. \tag{18}$$

where $l\#$ denotes the layer indices, with each layer's variables spanning $4N$ rows. For the k formulation of the multilayer, Eq. (17) can be stacked up in the same way. Thus far the analytical wave equation (9) is fully described by the discretized numerical forms, ready for the SAW boundary conditions to be introduced.

3.3. Boundary and interface conditions

Here the classic SAW problem is considered, where the top surface of the multilayer is exposed in vacuum with free mechanical conditions and either open- or short-circuit electrical condition; the wave amplitudes diminish exponentially into the depth. The physical meanings of the boundary and interface conditions are explained from top layer to bottom, and are implemented into the SCM model using the ω formation (Eqs (14) and (18)) as an example.

On the top surface, the free mechanical condition requires the normal surface stress components T_{i3}, which are calculated via Eq. (8), to be 0. This translates to the numerical relations of:

$$\left[(-ik)\Gamma^{31} + \Gamma^{33}\mathbf{Diff}\right]\mathbf{U}|_{l1} = \mathbf{0} \tag{19}$$

to be satisfied on the 1st, N + 1st and $2N$ + 1st rows in Eqn (18), which can be easily achieved by replacing these rows of $\mathbf{L}|_{l1}$ with those of the $\left[(-ik)\Gamma^{31} + \Gamma^{33}\mathbf{Diff}\right]$ matrix, and setting these rows of $\mathbf{M}|_{l1}$ as all 0.

If the electrical condition at the top surface is shorted, the physical relation is simply:

$$\phi = 0 \tag{20}$$

which is easily implemented into the $3N$ + 1st row of Eq. (18) by setting the $3N$ + 1st element of $\mathbf{L}|_{l1}$ as 1 and every other element on that row in $\mathbf{L}|_{l1}$ and $\mathbf{M}|_{l1}$ as 0. For an open-circuit top surface, the normal electrical displacement D_3 is continuous from the top layer of the medium to the vacuum above it. The electrical potential ϕ in the vacuum needs to satisfy the Laplace equation, and it was shown [10] that the solution gave the physical relation of:

$$D_3 = -\epsilon_0\frac{\partial\phi}{\partial x_3} = -\epsilon_0 k\phi, \text{ when } x_3 \le 0 \tag{21}$$

which, at $x_3 = 0$, should be equal to D_3 in the top layer calculated from Eq. (8). Therefore this electrical boundary condition is described by:

$$\left[k(\epsilon_0 - \mathrm{i}\Gamma^{31}) + \Gamma^{33}\mathbf{Diff}\right]\mathbf{U}|_{l1} = \mathbf{0} \tag{22}$$

which, like the short-circuit condition, is easily implemented to Eq. (18) through manipulations of its $3N$ + 1st row. Thus the conditions for the top surface are fully set by Eq. (19) combined with either Eq. (20) or (22).

Now consider the interfaces between layers, and take the one between layers 1 and 2 as an example. 6 mechanical (u_1, u_2, u_3, T_{13}, T_{23} and T_{33}) and 2 electrical (ϕ and D_3) variables are all required to be continuous across the interface. Focussing on u_1, the rows corresponding to its value at the interface are the Nth (bottom of the 1st layer) and $4N$ + 1st (top of the 2nd) in Eq. (18), and they are used to specify both u_1 and T_{13} continuities. For the u_1 across interfaces:

$$u_1|^{l1}_{\text{bottom}} - u_1|^{l2}_{\text{top}} = 0, \tag{23}$$

one only needs to set the Nth and $4N$ + 1st elements in the Nth row of the $\mathbf{L}$ matrix as 1 and −1, respectively, and set every other element of the row in $\mathbf{L}$ and $\mathbf{M}$ as 0. The T_{13} continuity is then similarly specified on the $4N$ + 1st row, with their numerical values calculated from Eq. (8):

$$\left[(-ik)\Gamma^{31} + \Gamma^{33}\mathbf{Diff}\right]|^{l1}_{\text{bottom}} - \left[(-ik)\Gamma^{31} + \Gamma^{33}\mathbf{Diff}\right]|^{l2}_{\text{top}} = \mathbf{0} \tag{24}$$

All the other physical variables at the interface can be similarly specified in pairs, including the electrical variables ϕ and D_3. These treatments are also equally applicable to every other interface of the multilayer. In practice, one may occasionally encounter interfaces that are shorted. In this case, all the mechanical variables are still continuous, but the electrical condition should be $\phi = 0$ on both sides of the interface, and D_3 - which needs not to be specified - may not be continuous any more.

Now that all the other interfaces are set, only the bottom of the multilayer remains to be dealt with. Since the amplitudes of the classic SAW decay exponentially into the medium, if the thickness is large enough (e.g. >2 × wavelength), then a simple clamped boundary condition (u_1, u_2, u_3 and ϕ all equal to 0) at the bottom surface is sufficient, and is extremely easy to implement into the SCM. Physically, this boundary condition is similar to modelling Lamb waves in the top half of the plate in large *fd* regions, where the A0 and S0 modes overlap and are both equivalent to the Rayleigh wave. Given its exponential decay with depth, neither the Perfect Matched Layer (PML) [19] nor the Laguerre polynomials [23] employed specifically for modelling SAWs in an infinite half space were in fact necessary.

3.4. Solution to the numerical wave equation

Both the ω and k formulations of the wave equation are expressed as a classic eigenvalue problem, and the introduced SAW boundary conditions have all maintained the linearity. Therefore, it can be easily solved by an eigensolver, such as the `eig` function in Matlab package via a simple command `eig(L,M)`, to obtain either ω or k as the eigenvalue, and the corresponding displacement vector $\mathbf{U}$ as the eigenvector together. Since the variables of $\mathbf{u}$ in each layer are directly accounted for at the interpolated collocation points, no exponential partial waves enter the equation, and the SCM is numerically unconditionally stable without requiring re-alignments of the partial waves needed by the recursive methods [18,19].

After the eigenvalues are obtained, the SAW phase velocity is calculated as $v_p = \omega/k$. Multiple solutions of the eigenvalue are given at once, which correspond to all modes of guided waves (not just SAWs) that satisfy the prescribed boundary conditions. Therefore the iterative root-finding process is no longer required and it is guaranteed that no mode is missed [24]. Spurious results exist in the obtained v_p values, which are often with erroneously large imaginary parts and should be rejected outright (when setting up the rejection, be careful that the true SAWs may also have a small imaginary part, normally in the order of $<10^{-6}$, due to numerical errors). True SAW modes require only minimal efforts to be selected from the remains, since they always have the lowest v_p of all guided wave modes (see, for example [29], about filtering of these modes). The eigenvector

U contains amplitude profiles of the variables into the depth, which also provides a double check to ensure correct SAW modes are selected.

Similar to the TMM, the SCM requires appropriate units for the physical variables to ensure its matrices are well-conditioned, because the Γ matrices contain tensor values of sharply contrasting amplitudes if the standard SI units are used, e.g. elastic stiffnesses are in the orders of 10^{11} Pa, while electrical permittivity is 10^{-12} F/m. The units suitable for the setup in this study are attached in the Appendix.

4. Example and results

The well-studied ZnO(001)/diamond/Si multilayer structure (Si as substrate) [32–35] is analysed here as an example to demonstrate the proposed SCM approach. This multilayer structure is of wide interests in high frequency telecommunications, since diamond offers the highest wave velocities of all materials. Material properties are cited from Ref. [32], and other common layered structures, such as AlN/diamond/Si, SiO2/LiNbO3 and ZnO/SiO2/Si, can be similarly analysed.

Physically, SAWs are introduced into the medium through the IDT coupled with the piezoelectric layer. Depending on the positioning of the IDT and a negligibly thin metal layer used to short-circuit an interface, there are four common configurations of the system, as shown in Fig. 2. The mechanical boundary conditions are the same for all these configurations, but the electrical conditions are different, resulting in different SAW performances.

Fragments of these performances have been covered in Refs. [19,32–35], using mainly the root-finding methods. Here a comprehensive examination of all these configurations' key SAW parameters is given via the SCM, including phase velocity and mode shapes, electromechanical coupling coefficients and effective permittivity. The accuracy of the results is calibrated against literature when available, and the SCM's advantages over the conventional methods are highlighted through specific demonstrations. Apart from the comprehensiveness in the case of piezoelectric media, the reader is also reminded of the generality of the SCM formulation, which can be easily adjusted to accommodate both elastic and magneto-electro-elastic materials, while previously these systems had to be pursued individually and laboriously.

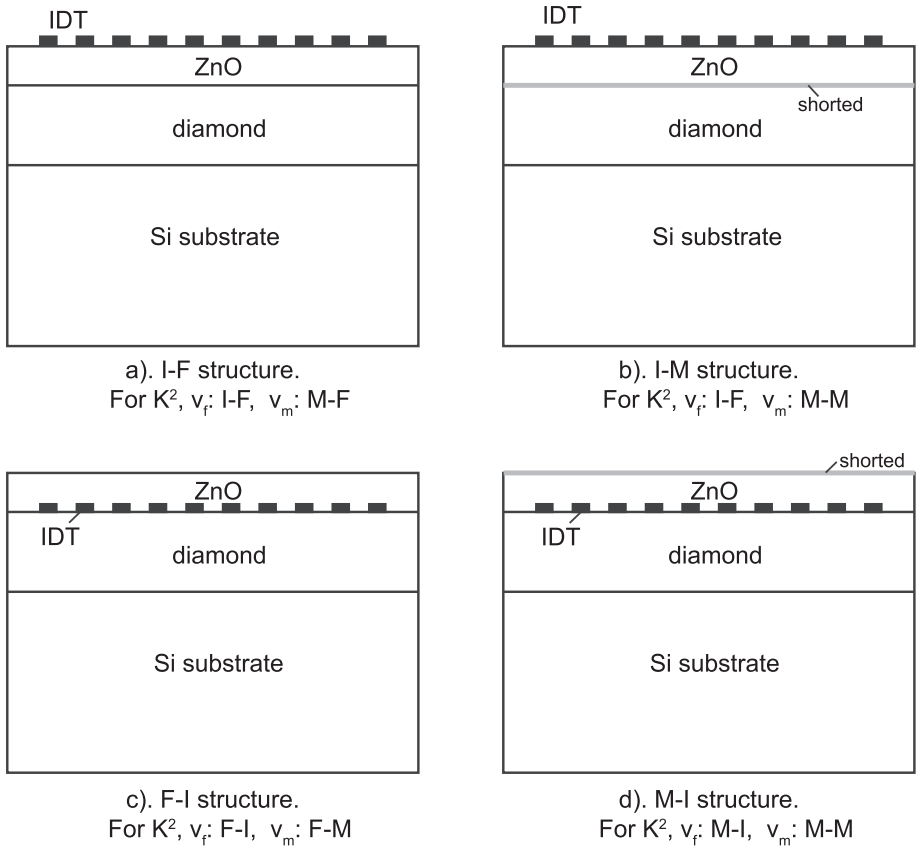

Fig. 2. Four possible configurations of the ZnO(001)/diamond/Si multilayer. Here I means IDT, M metalized (shorted), and F free (open-circuit). These configurations all have the same mechanical boundary conditions (free at the top and continuous at interfaces) but different electrical ones, leading to different SAW performances (e.g. the electromechanical coupling coefficient K^2, and the required conditions for its calculation is also listed).

4.1. Phase velocity dispersion curve and physical displacements

Phase velocity is the primary factor to consider when designing a SAW device. For the I-F configuration in Fig. 2, the velocity dispersion curves of the first three SAW modes are plotted in Fig. 3a, with the kH_{ZnO} value as the horizontal axis. They are calculated using $N = 50$ nodes to ensure both efficiency and accuracy (empirically, $\sim 10^{-5}$ relative error could be achieved with $N > 70$ for the first a few guided modes in a plate [24,26]; here only these first modes are sought-after, and the SCM models only the top half the plate, so similar accuracy is expected with a smaller N). The simultaneously obtained discretized displacement vector **U** are also plotted in Fig. 3(b–d) for three kH_{ZnO} locations to help identify the SAW modes. The mode with mostly the lowest speed has both u_1 and $u_3 = 0$ while $u_2 \neq 0$, hence is a shear-horizontal (SH) wave, or the Love mode, and it satisfies the boundary conditions because the top ZnO layer's (001) orientation allows decoupled SH waves. Both the other modes have $u_2 = 0$ and decaying u_1 and u_3 with depth; the slower one is the conventional Rayleigh wave, and the faster one is the Sezawa mode, which appears because the top ZnO layer has slower wave speeds than the diamond layer below. Most applications of diamond film-based SAW devices are based on the Sezawa mode [36] since it is lossless as the Rayleigh mode, but has higher velocities.

These dispersion curves are generated by varying k with H_{ZnO} fixed. Towards the lower end of the axis where $kH_{ZnO} \to 0$, the two higher modes have cut-off upper limits set by the top two layers' Rayleigh and shear velocities. Note that there are ambiguities to this end: if k is kept fixed with H_{ZnO} varying, the SAW speeds should effectively approach the limits of diamond since $H_{ZnO} \to 0$, as shown in Refs. [34,35] with a ZnO layer on an assumed diamond half space. Nonetheless, the SCM can handle both treatments, and this kH_{ZnO} region is not of major interests since it corresponds to either extremely thin layers or low wave frequencies.

As kH_{ZnO} grows, velocities of all three modes decrease as the waves are growingly influenced by the ZnO layer of lower speeds. At $kH_{ZnO} \approx 1.25$, the Rayleigh and Sezawa modes have very close velocities, but they do not cross. The vicinity of this region exemplify a difficult case for the root-finding methods (including scattering matrix and RASM) because: 1. The closeness between the two roots means that it is easy to miss one of them; 2. The kissing modes are difficult to identify correctly. In fact, in both [32,33], the inaccurately found roots led to the conclusion that the two modes did cross, resulting in subsequent

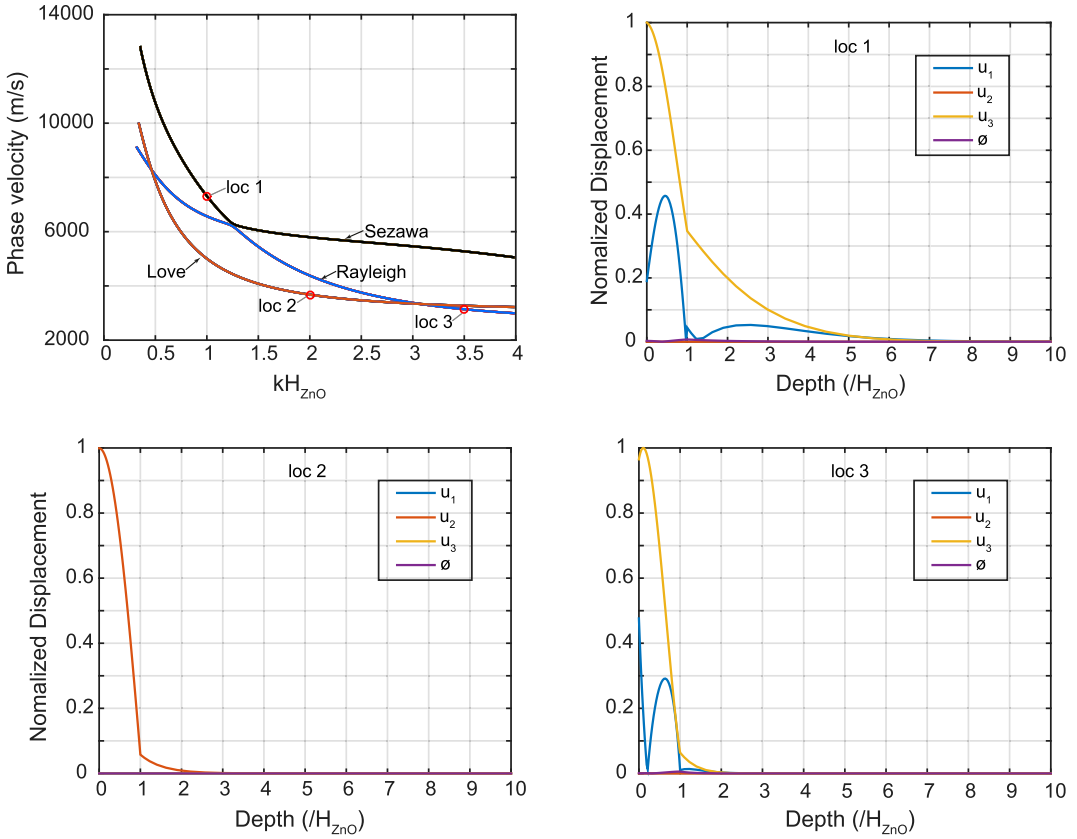

Fig. 3. Phase velocity dispersion curves and wave displacement vectors of the I-F configuration ZnO(001)/diamond/Si multilayer. a).Dispersion curves of the lowest 3 modes satisfying the boundary conditions, identified as Love, Rayleigh and Sezawa waves, respectively; b-d).Wave displacement amplitudes into the depth of the medium. The horizontal axes are the times of the ZnO layer thickness; all values calculated using three layer setup of thicknesses: ZnO-1 μm, diamond-22 μm and Si-30 μm, but only the starting region into the depth is plotted, since all values are all 0 beyond it. The diamond layer represents the typical large *fd* problem and shows the stability of the SCM.

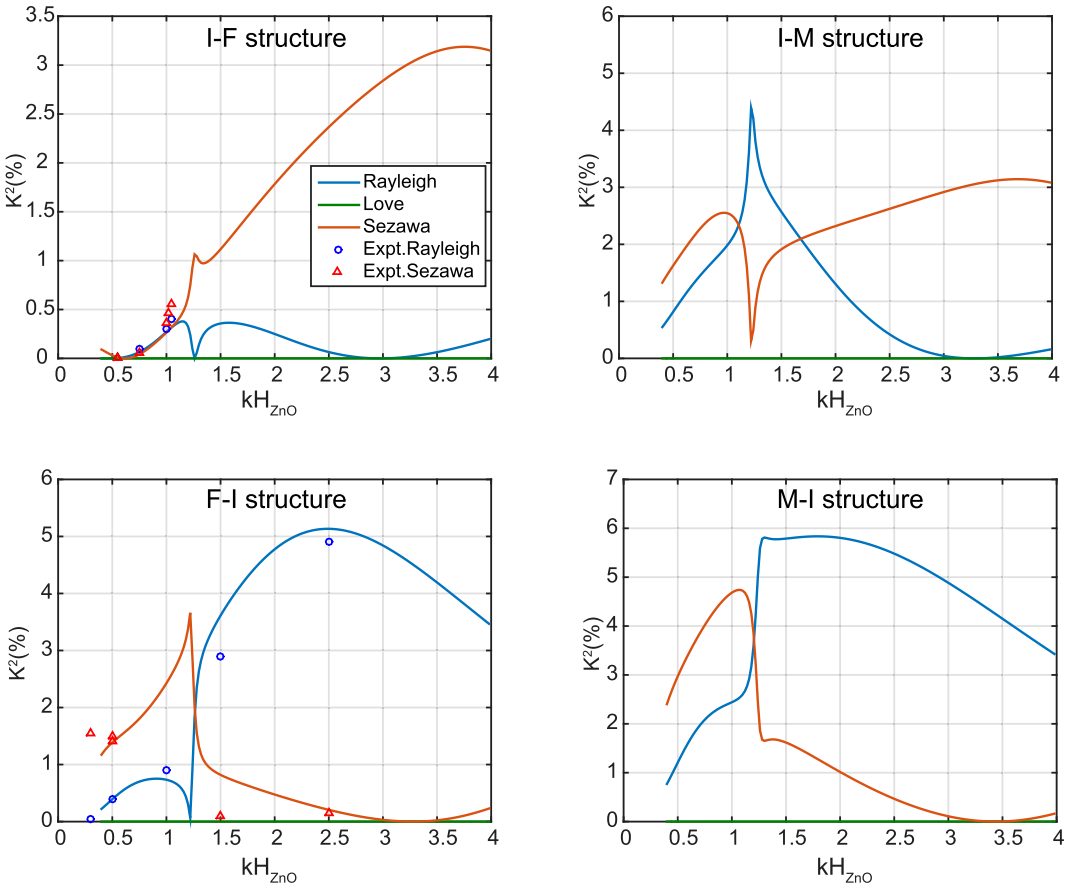

Fig. 4. K^2 amplitudes for the four multilayer configurations in Fig. 2. Same legends are used for all plots. The calculation is based on Ingebrigtsen approximation, which requires a pair of SAW velocities when the interface coupled with the IDT is both free and shorted, and the experimental results were reported in Ref. [32]. The pair needed for each configuration is also listed in Fig. 2.

erroneous calculations of K^2 and choices of modes [34]. In contrast, the SCM's calculation of all eigenvalues guarantees that no mode is missed, and the simultaneously obtained displacement profiles, which should be consistently changing for the same mode (e.g. the displacement u_1 has a $u_1 = 0$ node in the ZnO layer for the Rayleigh mode, but not for Sezawa), ensure easy mode identification.

Finally, when $k\mathrm{H}_{\mathrm{ZnO}}$ is large enough (e.g. >2.5), the SAW wavelength become shorter and the energy is mostly trapped in the top ZnO layer, hence their speeds eventually approach the guided wave speeds in ZnO. The association between phase velocity and wave motions into the depth is evident in the displacement plots in Fig. 4. The SAWs stretch well into the diamond layer when $k\mathrm{H}_{\mathrm{ZnO}} = 1.0$, but are evidently confined in ZnO when $k\mathrm{H}_{\mathrm{ZnO}} = 3.5$ as deducted. These observations show that the wave motions are well preserved into the first two layers, so only the ZnO/diamond layers are sufficient for modelling the SAWs for these thicknesses, no Si substrate is needed. However, the numerical stability of the SCM is emphasized here, since the diamond layer in all these cases is an exact example of the large *fd* problem that is problematic for the conventional TMM if a three-layer setup is used, but they can be easily handled by the SCM.

4.2. *The electromechanical coupling coefficient K^2*

The electromechanical coupling coefficient K^2 measures a piezoelectric medium's efficiency in converting applied electrical source into acoustic energy, and is another vital parameter for all types of SAW applications [5]. Various definitions of K^2 exist in the literature, but the most widely used one is based on the Ingebrigtsen approximation [37]:

$$K^2 = \frac{2\Delta v}{v_f} = \frac{2(v_f - v_m)}{v_f} \tag{25}$$

where v_f and v_m are the respective SAW velocities when the interface on which the IDT is placed is free or shorted. This definition, often called the $2\Delta v/v$ estimation, is also experimentally practical since the involved variables are relatively easy to observe from tests [5]. K^2 is normally shown as percentage.

Calculating K^2 through Eq. (25) apparently depends on the positioning of the IDT to determine which v_f and v_m to compare, which are listed in Fig. 2 for each of the configuration. The results for all four configurations are shown in Fig. 4, and the Rayleigh and Sezawa results agree with the theoretical and experimental results reported in Ref. [32]. In the vicinity of $k\mathrm{H}_{\mathrm{ZnO}} \approx 1.25$, the sharp fluctuations and local extrema of the K^2 is caused by the sudden bend of phase velocity evident in Fig. 3. As mentioned earlier, it is important to be clear that the dispersion curves do not cross, since this decides the correct choice of modes according to the favourable K^2 performances across $k\mathrm{H}_{\mathrm{ZnO}}$ regions.

As for the Love mode, the K^2 value is constantly 0 for all configurations, meaning that it cannot be directly excited or detected by the IDT. This is reasonable given that the SH wave is decoupled from other partial waves and piezoelectricity in the ZnO(001) layer; however, it has been shown both theoretically and experimentally [38,39] that for orientations such as (110) or (200) in ZnO, the SH modes have K^2 values as high as 3.5 and can be excited effectively (In fact, Love mode sensors are widely used in chemical or biochemical sensing because of their minimal energy loss in liquids [39] thanks to the lack of normal displacements). The important point here is that the SCM model is fully capable of capturing the characteristics of the SH modes, and can be used for their analyses.

Another important issue about K^2 is the confusion on whether to calculate it against $k\mathrm{H}_{\mathrm{ZnO}}$ (as has been done in Fig. 4, or equivalently $\mathrm{H}_{\mathrm{ZnO}}/\lambda$), or against $f\mathrm{H}_{\mathrm{ZnO}}$, since the two approaches can lead to significantly different results. For example, it was reported [34] that for the M-I configuration of the ZnO/diamond/Si system, calculating against $f\mathrm{H}_{\mathrm{ZnO}}$ yielded K^2 values of 25%, four times as large as against $k\mathrm{H}_{\mathrm{ZnO}}$. Such difference is caused by the SAW velocity dispersion in a layered structure: for a non-dispersive piezoelectric half space (which Eq. (25) was defined upon [37]), both assumptions end up with the same v_f and v_m regardless of the ω or k chosen; in a dispersive multilayer, on the other hand, for a particular combination of ω and k that gives a v_f, the corresponding v_m very much depends on whether to keep the same ω or k in the latter calculation. Even though Wu et al. [35] demonstrated that the discrepancies can be reconciled by using exact analytical calculations, the algorithm is difficult to compute and does not have connection to the practically measurable values of v_f and v_m. Fortunately, experimental results across many material systems (e.g. ZnO/diamond/Si [33], ZnO/SiO2/Si [38,39] and AlN/diamond [36]) predominantly show good agreement with the kH calculation, therefore this convention is recommended and the simple experimental evaluations of K^2 via v_f and v_m can be safely used.

4.3. Effective permittivity of multilayers

The effective permittivity ϵ_{eff} is a key concept for a piezoelectric material, providing a powerful tool for analyzing wave energy flow and electrode internal reflectivity, etc., and both phase velocity dispersion and K^2 can be obtained from ϵ_{eff}. For the I-F configuration, it is defined as:

$$\epsilon_{\mathrm{eff}} = \frac{D_{3-} - D_{3+}}{k\phi|_{x=0}} = \epsilon_0 - \frac{D_{3+}}{k\phi|_{x_3=0}} \tag{26}$$

where the solution to electrical potential in the vacuum half space (Eq. (21)) has been used. It is a complicated function of the slowness k/ω, and it describes electrical behaviours of the interface between vacuum and the ZnO layer.

One fundamental idea of finding ϵ_{eff} is to solve the eighth-order analytical wave equation with free mechanical yet unspecified electrical boundary condition, enabling the values of D_3 and ϕ to be found for any arbitrarily given slowness. Equivalently, ϵ_{eff} can also be obtained from the matrix-formed SAW Green's equation, e.g by using the guaranteed-stable scattering matrix [18] or RSAM [19] methods, though they require the recursive alignment of the growing and decaying partial waves in each layer of the system.

The SCM transforms the former idea into extremely simple manipulations of linear matrices. For the calculation in Eq. (26), the required unknown variables are D_{3+} and ϕ when $x_3 = 0$. The former is accessible via the numerical relation $\left[(-ik)\Gamma^{31} + \Gamma^{33}\mathbf{Diff}\right]\mathbf{U}|_{l1}$ (from analytical Eq. (8)) if the displacement vector $\mathbf{U}|_{l1}$ is known, while $\phi|_{x_3=0}$ is simply the $3N + 1$st element of $\mathbf{U}|_{l1}$, therefore ϵ_{eff} is set once $\mathbf{U}|_{l1}$ is found. This can be achieved considering the numerical wave equation for the multilayer (Eq. (18)), which requires the all-layer vector $\mathbf{U}$ satisfying:

$$\left(\mathbf{L} - \omega^2\mathbf{M}\right)\mathbf{U} = \mathbf{0} \tag{27}$$

where $\mathbf{L}$ and $\mathbf{M}$ are both with free mechanical surface conditions implemented while the electrical condition is left unspecified, and both k and ω are known for a given slowness. Apparently $\mathbf{U}$ is in the nullspace of the matrix $\left(\mathbf{L} - \omega^2\mathbf{M}\right)$, and it can be proved to be the only member there (fully specified boundary conditions does not have a solution for an arbitrary slowness unless it corresponds to a legitimate SAW mode, while relaxing only the surface electric condition allows one solution). It thus becomes almost a trivial step to obtain the $\mathbf{U}$ (in Matlab via the command `nullspace`) and ϵ_{eff} thereafter.

The ϵ_{eff} results for the I-F setup is plotted in Fig. 5, and they agree well with the exact results. Its connections to the SAW velocities are also easily found from the plot: the intersections of the curve with the horizontal axis correspond to $\epsilon_{\mathrm{eff}} = 0$ and $D_{3-} = D_{3-}$, so are solutions to the open-circuit electrical condition; the points where $\epsilon_{\mathrm{eff}} \to \infty$ are equivalent to $\phi|_{x_3=0}$, hence are solutions to the shorted condition. Consequently, K^2 can also be calculated by evaluating ϵ_{eff} (though beware that v_m from $\epsilon_{\mathrm{eff}} \to \infty$ can be inaccurate from the root-finding process for obvious reasons).

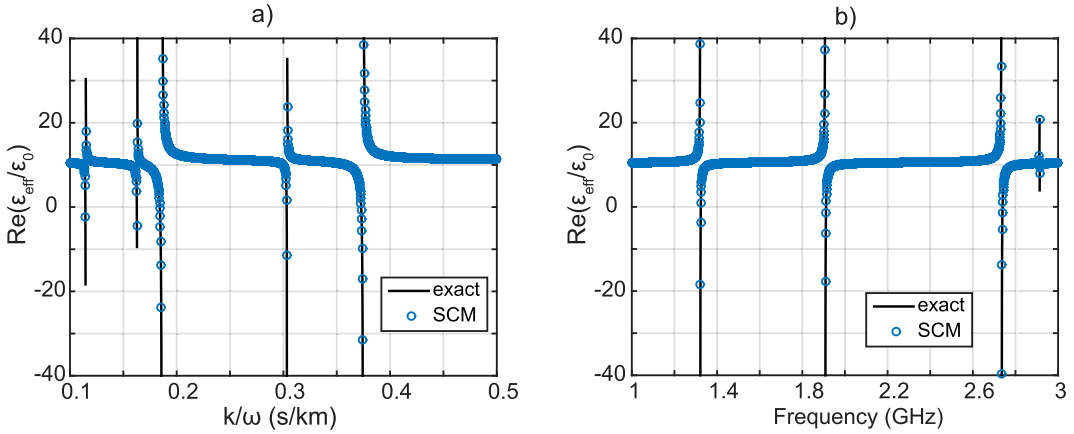

Fig. 5. Comparison between effective permittivity results of ZnO/diamond calculated by exact methods and SCM. Thicknesses are: ZnO-2 μm, diamond-30 μm. a). against slowness, frequency is 2.5 GHz; b). against frequency, phase velocity is 8 km/s. These settings are chosen to reproduce Fig. 2 in Ref. [19].

4.4. Discussions

In this simple example, the SCM has already demonstrated various advantages: it requires minimal efforts to formulate and code, and delivers all modes at once without missing any; it obtains wave motion profiles simultaneously to aid mode identification; and it is unconditionally stable and highly accurate. Thus it presents an attractive alternative to the root-finding approach in the analysis of SAWs across various types of materials. Furthermore, for certain circumstances where the root-finding approach does not work well, the SCM could bring even larger benefits. These include:

1. SAW in curved (cylindrical or spherical) coordinate systems. Ring waveguides and spherical SAW devices have emerged among other promising new developments in biosensing [40], and an example of a ball SAW sensor [41,42] is sketched in Fig. 6. With the SAW guided by a SiOx strip on the equator of a quartz crystal ball, the device demonstrated remarkable sensitivity to moisture. The SCM analysis of the SAW propagation should be based on the polar coordinates of Fig. 6b, where **r** and θ corresponds to x_1 and x_3 in Fig. 1; and the matrix expressions of the wave equation should be re-formulated in the similar fashion as introduced in Section 2.2, but using the curvilinear coordinate system given in Appendix 1 of [43]. However, such coordinate transformation is often not necessary, since high-frequency SAWs are normally used to avoid propagation interruption by geometries (160 MHz for ϕ1mm ball [41] and 80 MHz for ϕ3.3 mm [42]). This makes the wavelengths $\ll$ ball diameter, and the Cartesian system-based analysis in this paper remains adequate for these cases.
2. SAW in damping materials. Flexible electronics are growing into a huge industry. As fundamental building blocks of the technology, flexible SAW devices are normally achieved by depositing piezoelectric layers on polymers [44], which are often viscoelastic. This may add an imaginary part to the wavenumber, and the resultant two-dimensional root-finding process is much more difficult to achieve. The SCM, in contrast, solves the characteristic equation in exactly the same way with non-damping materials (now with complex Γ matrices), and deliver the complex wavenumbers directly.

On the other hand, the SCM is not without its own limits. Firstly, as discussed in Section 3, the SAW solutions are obtained as equivalences to the overlapping A0- and S0-mode guided waves in the large *fd* region, and this configuration could lead to

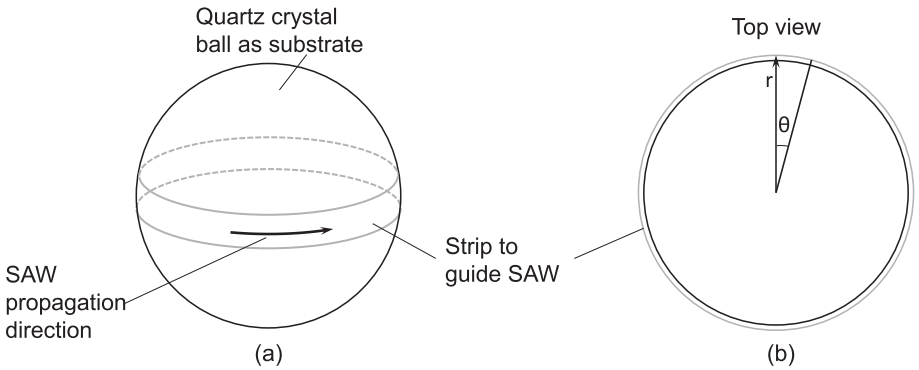

Fig. 6. Schematics of the ball SAW sensor developed in Refs. [41,42]. The SAW is guided by a SiOx strip on the equator of a quartz crystal ball.

spurious Lamb wave modes in the multilayers. Therefore one must examine the modal shapes (eigenvectors from the solver) carefully to sift out the correct modes that are in accordance to the SAW characteristics.

Moreover, the simple, clamped conditions at the lower boundary of the multilayer mean that the wave motions must be strictly decaying with depth, so the setup is not able to model the pseudo-SAW (also called the leaky SAW), which has a bulk-like partial wave with growing amplitude into the depth. It may seem that an absorbing layer (such as perfectly matched layer) combined with the SCM would provide a fix, but a series of complexities associated with the model (including the anisotropies of the medium, unorthodox wave equation formulations, and the grazing incidence of the leaky wave) make the formulation of a suitable absorbing layer extremely challenging and possibly inaccurate, and likely to deprive the characteristic simplicity from the SCM. Thus, the reader is recommended to resort to the root-finding methods for analysis on the pseudo-SAWs. However, it needs to be emphasized that the pseudo-SAWs are not a common phenomenon, but only appear on certain cuts of single crystals with relatively high crystal symmetries; besides, their propagations are intrinsically lossy with part of the energy radiated into the substrate. So they are not considered a major point of interest in piezoelectric multilayer designs, and certainly do not diminish the advantages and applicability of the SCM in the area.

5. Conclusions

This paper has established the SCM for the analyses of SAWs in piezoelectric multilayers. In Section 2 and 3, the governing equations of the wave propagation are deducted, reshaped into a matrix form, and then discretized by the SCM into two numerical formulations for direct calculations of either ω or k. They are both in the form of a classic eigenvalue problem, and can be easily solved to obtain the wanted velocity as the eigenvalue and the displacement vector as the eigenvector simultaneously. These solutions are equivalent to the A0 and S0-mode guided waves in the large fd region. The method is then applied on the well-studied ZnO/diamond/Si system, where the phase velocity dispersion relations, electromechanical coupling coefficients and effective permittivity are analysed, and the SCM results compared to existing techniques in literature. It is found that the SCM offers an intuitive, stable and accurate alternative to the conventional root-finding approach. Finally, some exciting potential applications of the SCM, as well as its intrinsic limits (e.g. on spurious modes and pseudo-SAWs), are discussed.

Acknowledgements

I am heavily indebted to Prof. Mike Lowe of Imperial College London for the help and advice during the preparation of the manuscript. I would also like to gratefully acknowledge Dr. Francisco Hernando Quintanilla and Prof. Richard Craster for much generous help on the topic of SCM. Helpful comments from Profs Lowe and Craster on the manuscript are much appreciated. This work is funded by the HexMat programme (EP/K034332/1) of the Engineering and Physical Sciences Research Council.

Appendix

Table A.1
Units used in the matrix method to mitigate the ill numerical conditions

	mass	length	time	frequency	density
SI	kg	m	s	Hz	kg/m^3
Here	10^{-12} kg	μm	10^{-9} s	GHz	10^6 kg/m^3
	velocity	acceleration	force	pressure	charge
SI	m/s	m/s^2	N	Pa	C
Here	10^3 ms^{-1}	10^{12} m/s^2	N	10^{12} Pa	10^{-12} C
	Voltage	piezoelectricity	permittivity		
SI	V	C/m^2	C/(V m)		
Here	10^6 V	C/m^2	10^{-12} C/(V m)		

References

[1] J.W. Strutt, On waves propagated along the plane surface of an elastic solid, Proc. Lond. Math. Soc. s1-17 (1885) 4–11.
[2] K. Aki, P. Richards, Quantitative Seismology, University Science Books, New York, 2002.
[3] Z. Zhou, K. Zhang, J. Zhou, G. Sun, J. Wang, Application of laser ultrasonic technique for non-contact detection of structural surface-breaking cracks, Optic Laser. Technol. 73 (2015) 173–178.
[4] J.-Y. Kim, S.I. Rokhlin, Determination of elastic constants of generally anisotropic inclined lamellar structure using line-focus acoustic microscopy, J. Acoust. Soc. Am. 126 (2009) 2998–3007.
[5] C. Campbell, Surface Acoustic Wave Devices for Mobile and Wireless Communications, second ed., Academic Press, 2007.
[6] K. Hashimoto, Surface Acoustic Wave Devices in Telecommunications: Modelling and Simulation, Springer Berlin Heidelberg, 2000.
[7] L.Y. Yeo, J.R. Friend, Surface acoustic wave microfluidics, Annu. Rev. Fluid Mech. 46 (2014) 379–406.
[8] F. Guo, Z. Mao, Y. Chen, Z. Xie, J.P. Lata, P. Li, L. Ren, J. Liu, J. Yang, M. Dao, S. Suresh, T.J. Huang, Three-dimensional manipulation of single cells using surface acoustic waves, Proc. Natl. Acad. Sci. U. S. A 113 (2016) 1522–1527.
[9] K. Länge, B.E. Rapp, M. Rapp, Surface acoustic wave biosensors: a review, Anal. Bioanal. Chem. 391 (2008) 1509–1519.

[10] G.W. Farnell, Properties of surface acoustic waves, in: W.P. Mason (Ed.), Physical Acoustics V6: Principles and Methods, Elsevier, 1970, pp. 109–166.
[11] W.T. Thomson, Transmission of elastic waves through a stratified solid medium, J. Appl. Phys. 21 (1950) 89–93.
[12] N.A. Haskell, The dispersion of surface waves on multilayered media, Bull. Seismol. Soc. Am. 43 (1953) 17–34.
[13] A. Fahmy, E.L. Adler, Propagation of acoustic surface waves in multilayers: a matrix description, Appl. Phys. Lett. 22 (1973) 495–497.
[14] E. Adler, Matrix methods applied to acoustic waves in multilayers, IEEE Trans. Ultrason. Ferroelectrics Freq. Contr. 37 (1990) 485–490.
[15] M.J.S. Lowe, Matrix techniques for modeling ultrasonic waves in multilayered media, IEEE Trans. Ultrason. Ferroelectrics Freq. Contr. 42 (1995) 525–542.
[16] L. Knopoff, A matrix method for elastic wave problems, Bull. Seismol. Soc. Am. 54 (1964) 431–438.
[17] B. Hosten, M. Castaings, Surface impedance matrices to model the propagation in multilayered media, Ultrasonics 41 (2003) 501–507.
[18] T. Pastureaud, V. Laude, S. Ballandras, Stable scattering-matrix method for surface acoustic waves in piezoelectric multilayers, Appl. Phys. Lett. 80 (2002) 2544–2546.
[19] L. Wang, S.I. Rokhlin, Recursive asymptotic stiffness matrix method for analysis of surface acoustic wave devices on layered piezoelectric media, Appl. Phys. Lett. 81 (2002) 4049–4051.
[20] I. Bartoli, A. Marzani, F.L. di Scalea, E. Viola, Modeling wave propagation in damped waveguides of arbitrary cross-section, J. Sound Vib. 295 (2006) 685–707.
[21] J. Lefebvre, V. Zhang, J. Gazalet, T. Gryba, V. Sadaune, Acoustic wave propagation in continuous functionally graded plates: an extension of the legendre polynomial approach, IEEE Trans. Ultrason. Ferroelectrics Freq. Contr. 48 (2001) 1332–1340.
[22] L. Elmaimouni, J.E. Lefebvre, V. Zhang, T. Gryba, A polynomial approach to the analysis of guided waves in anisotropic cylinders of infinite length, Wave Motion 42 (2005) 177–189.
[23] O. Bou Matar, N. Gasmi, H. Zhou, M. Goueygou, A. Talbi, Legendre and laguerre polynomial approach for modeling of wave propagation in layered magneto-electro-elastic media, J. Acoust. Soc. Am. 133 (2013) 1415–1424.
[24] A.T.I. Adamou, R.V. Craster, Spectral methods for modelling guided waves in elastic media, J. Acoust. Soc. Am. 116 (2004) 1524–1535.
[25] O.A. Peverini, R. Orta, R. Tascone, Analysis of piezoelectric strip waveguides based on the effective index and pseudospectral element methods, J. Acoust. Soc. Am. 112 (2002) 2623–2633.
[26] F. Hernando Quintanilla, M.J.S. Lowe, R.V. Craster, Modeling guided elastic waves in generally anisotropic media using a spectral collocation method, J. Acoust. Soc. Am. 137 (2015) 1180–1194.
[27] F. Hernando Quintanilla, M.J.S. Lowe, R.V. Craster, Full 3d dispersion curve solutions for guided waves in generally anisotropic media, J. Sound Vib. 363 (2015) 545–559.
[28] F. Hernando Quintanilla, M.J.S. Lowe, R.V. Craster, The symmetry and coupling properties of solutions in general anisotropic multilayer waveguides, J. Acoust. Soc. Am. 141 (2017) 406–418.
[29] F. Hernando Quintanilla, Z. Fan, M.J.S. Lowe, R.V. Craster, Guided waves' dispersion curves in anisotropic viscoelastic single- and multi-layered media, Proc. R. Soc. Math. A 471 (2015) 20150268.
[30] G. Coquin, H. Tiersten, Analysis of the excitation and detection of piezoelectric surface waves in quartz by means of surface electrodes, J. Acoust. Soc. Am. 41 (1967) 921–939.
[31] J.A. Weideman, S.C. Reddy, A matlab differentiation matrix suite, ACM Trans. Math Software 26 (2000) 465–519.
[32] H. Nakahata, A. Hachigo, K. Higaki, S. Fujii, S.-i. Shikata, N. Fujimori, Theoretical study on saw characteristics of layered structures including a diamond layer, IEEE Trans. Ultrason. Ferroelectrics Freq. Contr. 42 (1995) 362–375.
[33] H. Nakahata, S. Fujii, K. Higaki, A. Hachigo, H. Kitabayashi, S. Shikata, N. Fujimori, Diamond-based surface acoustic wave devices, Semicond. Sci. Technol. 18 (2003) S96.
[34] E.L. Adler, L. Solie, Zno on diamond: saws and pseudo-saws, in: Ultrasonics Symposium, 1995. Proceedings, vol. 1, IEEE, 1995, pp. 341–344.
[35] T.-T. Wu, Y.-Y. Chen, Exact analysis of dispersive saw devices on zno/diamond/si-layered structures, IEEE Trans. Ultrason. Ferroelectrics Freq. Contr. 49 (2002) 142–149.
[36] M. Benetti, D. Cannata, F. Di Pictrantonio, E. Verona, Growth of aln piezoelectric film on diamond for high-frequency surface acoustic wave devices, IEEE Trans. Ultrason. Ferroelectrics Freq. Contr. 52 (2005) 1806–1811.
[37] K.A. Ingebrigtsen, Surface waves in piezoelectrics, J. Appl. Phys. 40 (1969) 2681–2686.
[38] Z. Zhang, Z. Wen, C. Wang, Investigation of surface acoustic waves propagating in zno–sio 2–si multilayer structure, Ultrasonics 53 (2013) 363–368.
[39] J. Luo, A. Quan, C. Fu, H. Li, Shear-horizontal surface acoustic wave characteristics of a (110) zno/sio 2/si multilayer structure, J. Alloy. Comp. 693 (2017) 558–564.
[40] Z. Xu, Y.J. Yuan, Implementation of guiding layers of surface acoustic wave devices: a review, Biosens. Bioelectron. 99 (2018) 500–512.
[41] S. Hagihara, T. Tsuji, T. Oizumi, N. Takeda, S. Akao, T. Ohgi, K. Takayanagi, T. Yanagisawa, N. Nakaso, Y. Tsukahara, K. Yamanaka, Highly sensitive trace moisture ball surface acoustic wave sensor using sio x film, Jpn. J. Appl. Phys. 53 (2014) 07KD08.
[42] K. Takayanagi, S. Akao, T. Yanagisawa, N. Nakaso, Y. Tsukahara, S. Hagihara, T. Oizumi, N. Takeda, T. Tsuji, K. Yamanaka, Detection of trace water vapor using siox-coated ball saw sensor, Mater. Trans. 55 (2014) 988–993.
[43] B. Auld, Acoustic Fields and Waves in Solids, R.E. Krieger, 1990.
[44] H. Jin, J. Zhou, X. He, W. Wang, H. Guo, S. Dong, D. Wang, Y. Xu, J. Geng, J. Luo, J. Geng, W. Milne, Flexible surface acoustic wave resonators built on disposable plastic film for electronics and lab-on-a-chip applications, Sci. Rep. 3 (2013) 2140.